Appl. Phys. B (2014) 114:455–459
DOI 10.1007/s00340-014-5802-5

Applied Physics B
Lasers and Optics

RAPID COMMUNICATION

Intensity vibration sensor based on Raman fiber laser using a distributed mirror combined with Bragg grating structures

H. F. Martins · M. B. Marques · O. Frazão

Received: 8 November 2013 / Accepted: 11 February 2014 / Published online: 20 February 2014

Abstract In this work, the authors propose a new configuration for an intensity vibration sensor based on a Raman fiber laser. The linear cavity of the Raman fiber laser relies on the combination of a distributed Rayleigh mirror and fiber Bragg gratings, which are used as the sensing element and intensity filter. The sensor was able to measure vibrations with frequencies of up to 350 Hz with more than 50 dB of signal-to-noise ratio (SNR) and also the amplitude of the vibrations with a sensitivity of up to 0.57 ± 0.07 dB/με for vibrations with a maximum strain variation of up to 35 με. The main advantages of the proposed configuration are the simple scheme with high SNR for remote sensing and the easy possibility of multiplexing.

1 Introduction

Raman fiber Bragg grating (FBG) lasers using a linear cavity have been widely researched and improved in the last two decades [1]. Recently, ultralong Raman fiber lasers (URFL) have been implemented as very attractive solutions for optical communication links [2]. Although fiber lasers based on the Raman effect can present some restrictions when high power is injected in the fiber due to the gain suppression created by the Rayleigh scattering growth, systems where power losses are continuously compensated using second-order Raman pump, creating virtually lossless fiber spans, have been demonstrated [3]. The principle was used to demonstrate a resolvable mode structure of an URFL with a 270 km cavity in 2009 [4]. Rayleigh scattering can also be used as a distributed random mirror to enhance the generation of Brillouin–Raman comb lasers [5–8], multiwavelength generation [9, 10] and random distributed lasers [11]. In 2010, a 200-km-dual-wavelength URFL using two FBGs with different wavelengths, one on each side of the fiber span, was reported [12]. The laser cavities of the two independent Raman fiber lasers were formed between the FBGs and a distributed random mirror created by Rayleigh scattering, resulting in laser action with the same wavelength of the FBG.

In optical sensing, several sensors combining the use of FBGs with Rayleigh scattering have been reported. FBGs can be used as sensing heads for the measurement of strain, temperature or others physical parameters, since the variation of these parameters induces changes on the central Bragg wavelength [13, 14]. Recently, a temperature-insensitive strain sensor using two different wavelength Raman FBG lasers which used cooperative Rayleigh scattering was reported [15]. The use of Raman fiber lasers also allows for remote optical sensing. Recently, a 300-km URFL (with cooperative Rayleigh scattering) using a distributed mirror was reported for sensing applications [16]. Also, a new method to extend the range of Brillouin optical time domain analysis systems for up to 100 km with submeter resolution was reported [17]. The work exploits the virtual transparency created by second-order Raman pumping in optical fibers.

Conventional vibration sensors, based on capacitive or piezoelectric principles, can present performance

H. F. Martins (✉) · M. B. Marques · O. Frazão
INESC Porto, Rua do Campo Alegre, 687,
4169-007 Porto, Portugal
e-mail: hfm@inescporto.pt

M. B. Marques
e-mail: mbmarque@fc.up.pt

O. Frazão
e-mail: ofrazao@fc.up.pt

H. F. Martins · M. B. Marques · O. Frazão
Faculdade de Ciências da Universidade do Porto, Rua do Campo Alegre, 687, 4169-007 Porto, Portugal

limitations due to the problem of electrical isolation, especially in the presence of high voltages and high magnetic fields [18, 19]. Optical fiber sensors, however, present several characteristics that make them particularly attractive when compared to traditional sensors, such as inherent immunity to electromagnetic interference, small size, possibility of remote operation and multiplexing capability. Furthermore, the fiber can be used as both the sensing element and the communication channel [20, 21].

Within the optical fiber sensors, a distinction can be made between passive FBG-based and active laser-based sensor systems. Passive FBG-based sensors rely on the simple reflection of light coming from a spectrally broadband source. In this case, the optical power of the signal to be detected is rather small as the FBGs present narrowband reflection spectra and no amplification occurs, which results in a low SNR. In the case of active laser-based sensors, however, the signal is amplified in the optical domain before being detected, rather than in the electronic domain after detection, which leads to a significant improvements in the SNR, especially in the presence of high background noise [22]. An improvement of up to 40 dB in the amplitude and 20 dB in the SNR of the detected vibrations between active (laser-based sensor) and passive devices (illuminating FBGs with a broadband source) under similar conditions has been demonstrated [23]. For remote sensing, considering the typical single-mode fiber losses, an increase of 40 dB in the amplitude of the signal would allow the sensing range to be increased by $\simeq 100$ km.

In this work, the authors present a new configuration for an intensity vibration sensor based on a Raman fiber laser. The linear cavity of the Raman fiber laser relies on the combination of a distributed Rayleigh mirror and FBGs, which are used as the sensing element and intensity filter.

2 Operation mode

Figure 1 presents the configuration of the Raman FBG laser intensity vibration sensor. The gain in this configuration is provided by a 1,455 nm Raman pump laser with a maximum power of 5 W which creates a typical broadband Raman gain in the dispersion compensating fiber (DCF) with a maximum around 1,555 nm (13.1 THz above the pump laser frequency). Two wavelength division multiplexers (1,450/1,550 nm) and a 1 km DCF with a dispersion coefficient of -132 ps nm^{-1} km^{-1} are used. In this configuration, a laser cavity is formed between two fiber Bragg gratings (FBG), which are also used as the sensing head and intensity filter. The process is assisted by a distributed mirror created by Rayleigh scattering in the DCF.

The sensing head is the sensor FBG and is connected to the rest of the setup by 10 km of SMF 28, to simulate a remote sensing configuration. In order to characterize the sensor FBG as a vibration sensor, it is attached to a piezoelectric element (PZT) in which vibrations with a frequency of up to 1 kHz can be applied using an electric modulator. The filter FBG is used as the intensity filter to interrogate the vibration applied to the sensor. In this case, the reflection spectra of the filter FBG and the sensor FBG are tuned to be partially overlapped. By properly tuning the Raman pump power, lasing can be set to only occur in the overlap of the reflection spectra of both FBGs. Due to the wavelength shift of the reflection spectrum of the sensor FBG induced by deformations (simulated by the PZT), the overlap of the reflection spectra of both FBGs will be higher when negative wavelength shifts are applied. The resulting laser spectrum will therefore have higher optical power and lower wavelength peak than when positive wavelength shifts are applied.

Finally, in order to monitor the optical power of the laser output, a photodetector was used to convert the laser output optical spectrum in an electrical signal which was then observed by an electric spectrum analyzer. Also, in parallel, an optical spectrum analyzer with a maximum resolution of 0.05 nm was used to observe the laser output optical spectrum. The optical power output as a function of the Raman power input of the Raman FBG laser was characterized without the filter FBG (Fig. 2). The threshold was observed to be at 350 mW and the linear regime observed in the range of 700–1,000 mW with a laser slope efficiency of 1.49 ± 0.05 %. The inset figure presents the output spectrum for the input Raman pump power of 600 and 800 mW. For higher pump powers, the central wavelength of the laser is shifted to higher wavelengths and the efficiency increases due to the Raman gain profile which has a maximum at 1,555 nm.

3 Experimental results

Using the experimental setup presented in Fig. 1, the output optical spectrum was observed when the maximum (15 V) and minimum (-15 V) voltages were applied to the PZT (Fig. 3). As expected, for the minimum applied voltage, the output spectrum had a higher optical power since the overlap of the reflection spectra of the FBGs is higher and the peak is placed at a lower wavelength. The inset figure of Fig. 3 presents the reflection spectra of both FBGs, which were measured with a FBG interrogator. The filter FBG presents a typical 100 % saturated FBG reflection spectrum, with a 0.23 nm full width at half maximum (FWHM) and centered at 1,549.98 nm, which drops 19 dB between 1,550.07 and 1,550.17 nm. As for the sensor FBG,

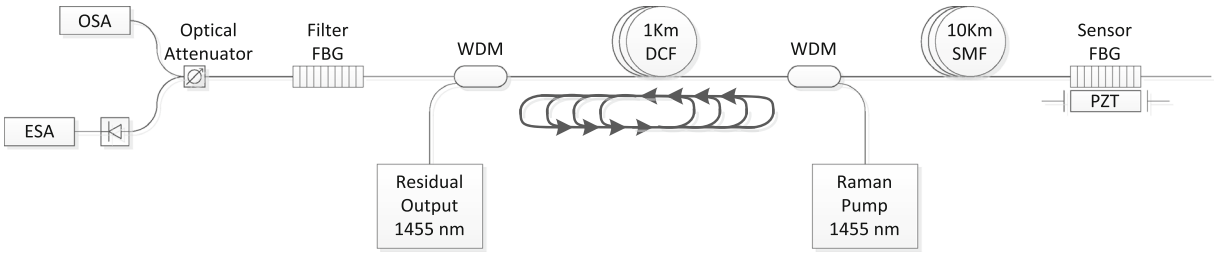

Fig. 1 Experimental setup of the Raman FBG laser intensity vibration sensor

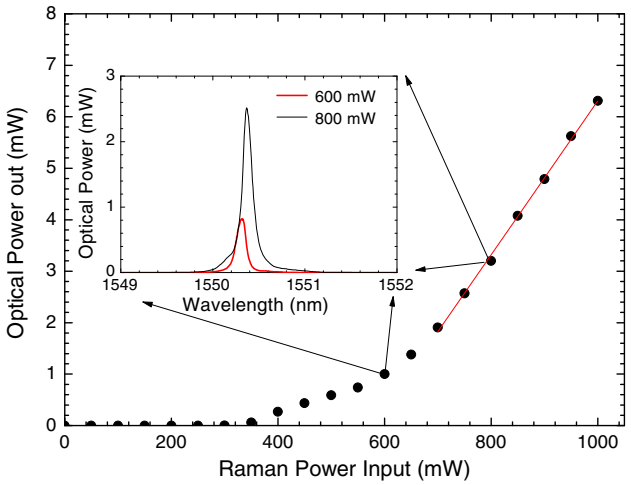

Fig. 2 Optical power output as a function of the Raman power input of the Raman FBG laser without the filter FBG (*Inset* fig.: output spectra for the input Raman pump power of 600 and 800 mW)

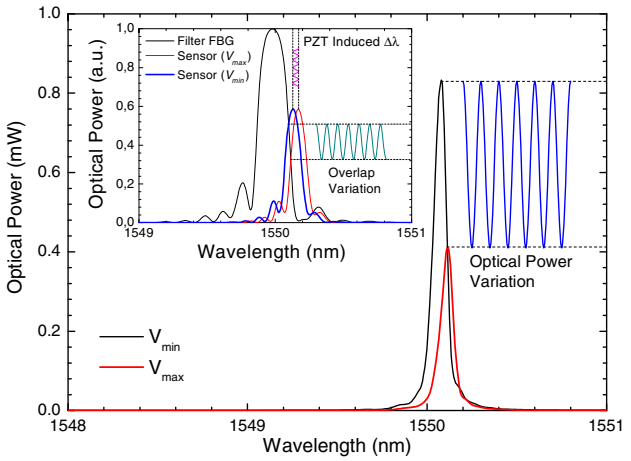

Fig. 3 Optical output spectra for maximum and minimum applied strain to the sensing head (*Inset* fig.: reflection spectra of the filter FBG and sensor FBG for maximum and minimum applied strain to the sensing head)

it presents a 60 % reflectivity and is centered at 1,550.13 nm for the minimum applied voltage on the PZT (−15 V) and at 1,550.17 nm for the maximum applied voltage (15 V). The sensor FBG has a 0.13 nm FWHM and

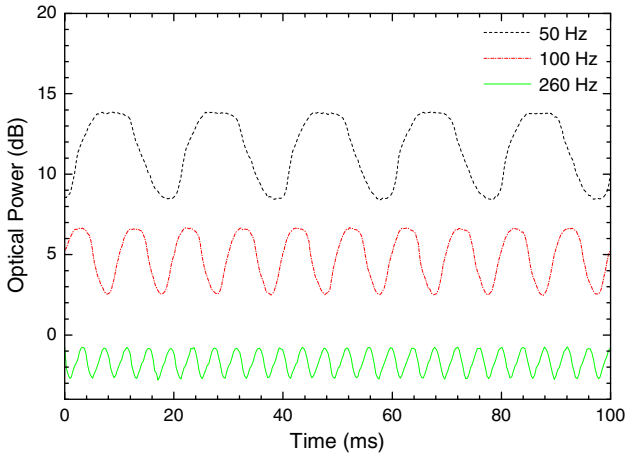

Fig. 4 Output optical power variation of the laser in the time domain for applied vibrations of different frequency (arbitrary optical power reference level)

drops 11 dB between the center and 1 nm away from the center.

A sinusoidal electric signal with 30 Vpp (varying between −15 and 15 V) was applied to the PZT and the output optical power was observed in the time domain for the frequencies of 50, 100 and 260 Hz (Fig. 4). A sinusoidal variation was observed as expected, with an amplitude that was observed to decrease with the frequency. An amplitude of 6.5 dB for 50 Hz, 5.2 dB for 100 Hz and 3.5 dB for 260 Hz was observed, and all spectra had a maximum optical power close to 0 dBm. The optical response was not perfectly sinusoidal due to insufficient pretension applied to the sensor FBG during the attachment to the PZT.

With the same electrical signal applied to the PZT, the optical power output signal was converted to an electrical signal. This signal was characterized in the spectral domain, and the amplitude of the central frequency was measured as a function of the frequency applied to the PZT (Fig. 5). The amplitude of the central frequency was observed to decrease with the applied frequency, decreasing 3 dB (with respect to the lower frequencies) at 200 Hz and having a steep decrease after 240 Hz. The signal-to-noise ratio (SNR) of the spectra for applied frequencies

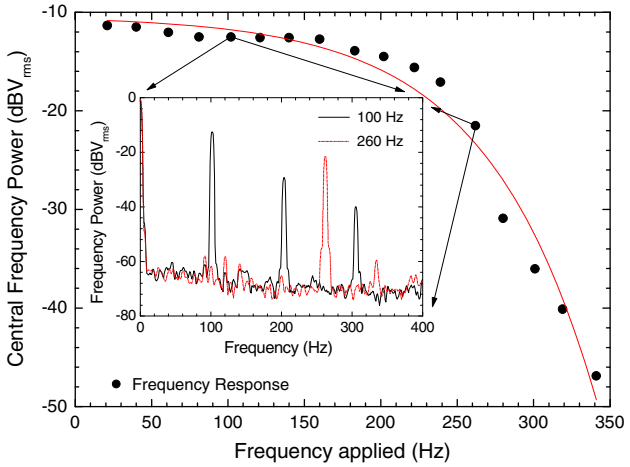

Fig. 5 Central frequency output power (converted electric signal) for applied vibrations of different frequencies (*Inset* fig.: output power in the frequency domain for 100 and 260 Hz)

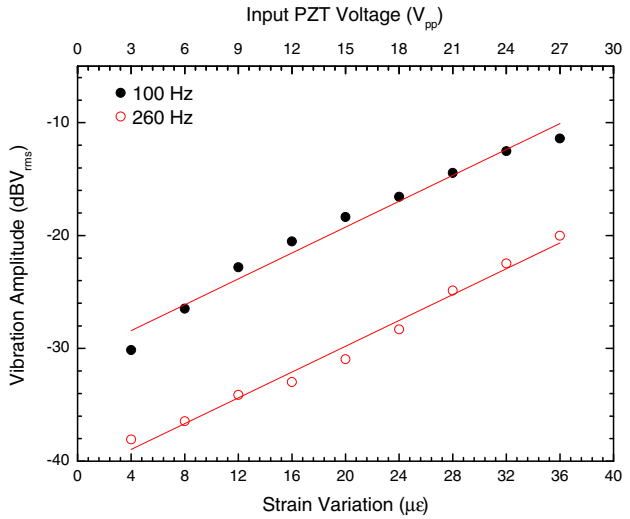

Fig. 6 Amplitude of the vibration as a function of the maximum strain variation (induced by applying an electrical signal to the PZT)

below 260 Hz was higher than 50 dB, and a well-defined frequency peak was observed for applied frequencies of up to 340 Hz, which had a 22 dBV_{rms} SNR. The inset figure presents the output power in the frequency domain for the case of an applied frequency of 100 and 260 Hz. Higher order harmonics (owned to insufficient pretension of the FBG, resulting in the clipped sinusoids of Fig. 4) are clearly observed for the case of the 100 Hz (at 200 and 300 Hz) but with lower amplitudes than the applied frequency. A 1/f noise was observed with an average power varying between -65 dBV_{rms} for frequencies near 0 and -70 dBV_{rms} for frequencies near 400 Hz.

The amplitude of the central frequency of the output spectrum was measured as a function of the maximum strain variation applied to the fiber (proportional to the maximum amplitude of the signal applied to the PZT), with a constant applied frequency (Fig. 6). Considering a perfect sinusoidal movement, the maximum acceleration will be given by: $Max_{acceleration} = Max_{strain} \times L_{FBG}/(2\pi f)^2$, where f is the frequency of the movement and L_{FBG} is the sensor FBG length (≈ 1 cm). A response with a sensitivity of 0.57 ± 0.07 dB/με $[2.3 \pm 0.3 \times 10^{13}$ dB/(ms^{-2})] for an applied frequency of 100 Hz and 0.57 ± 0.05 dB/με $[1.5 \pm 0.1 \times 10^{14}$ dB/(ms^{-2})] for an applied frequency of 260 Hz was obtained.

4 Discussion

In the presented intensity vibration sensor, the output power variation is due to the difference of overlap of the reflection spectra of the FBGs which creates a laser spectrum with a different power. When the overlap of the reflection spectra of the FBGs is higher (sensor FBG shifted to lower wavelengths), the output power is higher, even though the peak of the laser is placed in a wavelength with lower Raman gain (which increases with wavelength in the region where the FBGs are placed, having a peak at 1,555 nm). However, a higher power variation would be expected if the Raman gain was lower for higher wavelengths.

The fact that lasing occurs between the FBGs provides a higher SNR and also means that the output optical power to be measured will be higher than other schemes relying on simply measuring the optical power reflected by FBG. The sensor was able to measure frequencies of up to 350 Hz, being limited by the PZT response which had a resonance near that frequency. However, considering the laser cavity length ($\simeq 10^{-4}$ s for a light whole round-trip), measurements above 1 kHz are not expected. As for the remote sensing, 10 km were demonstrated but considering the power and SNR of the output signal, no problems are envisaged for distances of up to 100 km, although a maximum detectable frequency bandwidth decrease would be expected.

Temperature variations in the sensing head will shift the reflection spectra of the sensor FBG and could in principle interfere with the vibration measurement. In the typical case, however, the temperature variations will be much slower than the strain variations of the vibration to detect. Therefore, the temperature variations will not affect the vibration measurements if the temperature difference between the two FBGs is not too high (≈ 20 °C) in which case the reflection spectra of the FBGs would no longer overlap and vibration measurements would no longer be possible.

5 Conclusion

To our knowledge, the use of a Raman FBG laser for an intensity vibration sensor is reported for the first time. When vibrations were applied to the sensing head, a sinusoidal variation of the output power of the Raman fiber laser was observed with a maximum optical output power of 0 dBm and maximum amplitude of 6.5 dB. The sensor was able to measure vibrations with frequencies of up to 350 Hz and also the amplitude of the vibrations with a sensitivity of up to 0.57 ± 0.07 dB/με ($2.3 \pm 0.3 \times 10^{13}$ dB/(ms^{-2}) for 100 Hz) for vibrations with a maximum strain variation of up to 35 με (maximum acceleration of up to 9×10^{-13} ms^{-2} for 100 Hz). The frequency spectra were observed to have a SNR higher than 50 dBV_{rms} for frequencies below 250 Hz. Remote sensing in a distance of 10 km was simulated but no problems are envisage in distances of up to 100 km, although a maximum detectable frequency bandwidth decrease would be expected.

The presented configuration allows for a low cost interrogation of vibrations since the measured is optical power variation and high SNRs are achieved. The performance of the sensor could be improved by using higher quality FBGs and a different Raman gain profile.

Acknowledgments This work was supported by project NORTE-07-0124-FEDER-000058 is financed by the North Portugal Regional Operational Programme (ON.2—O Novo Norte), under the National Strategic Reference Framework (NSRF), through the European Regional Development Fund (ERDF), and by national funds, through the Portuguese funding agency, Fundação para a Ciência e a Tecnologia (FCT). H. Martins acknowledges a scholarship from FCT Fundação para a Ciência e a Tecnologia (Portuguese Foundation for Science and Technology), SFRH/BD/76991/2011.

References

1. G. Grubb, T. Strasser, W.Y. Cheung, W.A. Reed, V. Mizrahi, T. Erdogan, P.J. Lemaire, A.M. Vengsarkar, D.J. DiGiovanni, D.W. Peckham, B.H. Rockney, Osa. Trends Opt. Photo. **18**, 31 (1995)
2. J.D. Ania-Castanon, V. Karalekas, P. Harper, S.K. Turitsyn, Phys. Rev. Lett. **101**, 123903 (2008)
3. J.D. Ania-Castanon, T.J. Ellingham, R. Ibbotson, X. Chen, L. Zhang, S.K. Turitsyn, Phys. Rev. Lett. **96**, 023902 (2006)
4. S.K. Turitsyn, J.D. Ania-Castanon, S.A. Babin, V. Karalekas, P. Harper, D. Churkin, S.I. Kablukov, A.E. El-Taher, E.V. Podivilov, V.K. Mezentsev, Phys. Rev. Lett. **103**, 133901 (2009)
5. K.D. Park, B. Min, P. Kim, N. Park, J.H. Lee, J.S. Chang, Opt. Lett. **27**, 155–157 (2002)
6. B. Min, P. Kim, N. Park, IEEE Photonic. Tech. L. **13**, 1352–1354 (2001)
7. A.K. Zamzuri, M.I.M. Ali, A. Ahmad, R. Mohamad, M.A. Mahdi, Opt. Lett. **31**, 918 (2006)
8. S. Shahi, S.W. Harun, H. Ahmad, Laser Phys. Lett. **6**, 737–739 (2009)
9. A.M.R. Pinto, O. Frazao, J.L. Santos, M. Lopez-Amo, Appl. Phys. B-Lasers O. **99**, 391–395 (2010)
10. A.M.R. Pinto, O. Frazao, J.L. Santos, M. Lopez-Amo, J. Lightwave Technol. **29**, 1482–1488 (2011)
11. S.K. Turitsyn, S.A. Babin, A.E. El-Taher, P. Harper, D.V. Churkin, S.I. Kablukov, J.D. Ania-Castanon, V. Karalekas, E.V. Podivilov, Nat. Photonics **4**, 231–235 (2010)
12. A.E. El-Taher, M. Alcon-Camas, S.A. Babin, P. Harper, J.D. Ania-Castanon, S.K. Turitsyn, Opt. Lett. **35**, 1100–1102 (2010)
13. O. Frazao, L.A. Ferreira, F.M. Araujo, J.L. Santos, Fiber Integr. Opt. **24**, 227–244 (2005)
14. M.S. Ferreira, M. Becker, H. Bartelt, P. Mergo, J.L. Santos, O. Frazão, Laser Phys. Lett. **10**, 095102 (2013)
15. H.F. Martins, M.B. Marques, O. Frazao, Appl. Phys. B-Lasers O. **104**, 957–960 (2011)
16. H. Martins, M.B. Marques, O. Frazao, Opt. Express **19**, 18149–18154 (2011)
17. X. Angulo-Vinuesa, S. Martin-Lopez, P. Corredera, M. Gonzalez-Herraez, Opt. Express **20**, 12147–12154 (2012)
18. V. Demjanenko, R.A. Valtin, M. Soumekh, H. Naidu, A. Antur, D.P. Hess, A. Soom, M.K. Tangri, S.Y. Park, D.M. Benenson, S.E. Wright, IEEE T. Power Deliv. **7**, 656–663 (1992)
19. M. Runde, T. Aurud, L.E. Lundgaard, G.E. Ottesen, K. Faugstad, S.A. Boggs, IEEE T. Power Deliv. **7**, 1306–1314 (1992)
20. T.K. Gangopadhyay, Sensor Actuat. A-Phys. **113**, 20–38 (2004)
21. T.G. Giallorenzi, J.A. Bucaro, A. Dandridge, G.H. Sigel, J.H. Cole, S.C. Rashleigh, R.G. Priest, IEEE J. Quantum Elect. **18**, 626–665 (1982)
22. J. Mandal, Y. Shen, S. Pal, T. Sun, K.T.V. Grattan, A.T. Augousti, Opt. Commun. **244**, 111–121 (2004)
23. M.S. Ferreira, M. Becker, H. Bartelt, P. Mergo, J.L. Santos, O. Frazão, Laser Phys. Lett. **10**, 095102 (2013)